ACS APPLIED MATERIALS & INTERFACES

RESEARCH ARTICLE

www.acsami.org

Finely Tailored Performance of Inverted Organic Photovoltaics through Layer-by-Layer Interfacial Engineering

Qun Chen,[†,‡] Brian J. Worfolk,[†,‡] Tate C. Hauger,[†,‡] Usama Al-Atar,[†,‡] Kenneth D. Harris,[‡] and Jillian M. Buriak*[,†,‡]

[†]Department of Chemistry, University of Alberta, 11227 Saskatchewan Drive, Edmonton, Alberta T6G 2G2, Canada

[‡]National Institute for Nanotechnology, 11421 Saskatchewan Drive, Edmonton, Alberta T6G 2M9, Canada

Supporting Information

ABSTRACT: Control over interfacial properties in organic photovoltaics (OPVs) is critical for many aspects of their performance. Functionalization of the transparent conducting electrode, in this case, indium tin oxide (ITO), through an electrostatic layer by layer (eLbL) approach with cationic *N*,*N*′-bis[2-(trimethylammonium)ethylene] perylene-3,4,9,10-tetracarboxyldiimide ($PTCDI^+$) and anionic poly(3,4-ethylenedioxythiophene):poly(*p*-styrenesulfonate) ($PEDOT:PSS^-$), led to high control over the surface properties. The films were studied through a variety of surface and spectroscopic techniques, including X-ray photoelectron spectroscopy (XPS), UV−visible spectroscopy, atomic force microscopy (AFM), and ellipsometry. The work function of modified ITO was measured by UV photoelectron spectroscopy (UPS) and showed oscillating values with respect to odd−even layer numbers; the strong odd−even effect is due to the differing electronic characteristics of the top layer, either $PTCDI^+$ or $PEDOT:PSS^-$. The modified ITO electrodes were then used as the cathode in a series of inverted organic photovoltaic architectures. The performance of inverted OPVs was, in parallel to the UPS results, found to be highly dependent on the layer number of coated films and showed an obvious oscillation based on layer number. Inverted OPVs were retested after 128 days of storage in air, and almost all devices maintained over 70% of original power conversion efficiency (PCE).

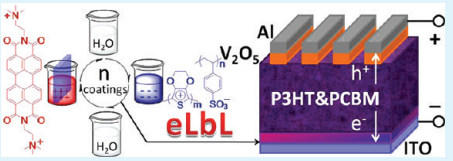

KEYWORDS: layer-by-layer, inverted organic photovoltaics, perylenediimide, interfacial engineering, odd−even effect

1. INTRODUCTION

Excitonic organic photovoltaics (OPVs) based upon the bicontinuous bulk heterojunction (BHJ) structure represent a promising solar cell technology with advantageous properties such as low cost production, device flexibility, and a customizable aesthetic appearance.[1−7] In these OPV devices, photon absorption within the photoactive material creates excitons, which then dissociate into holes and electrons at donor/acceptor interfaces. Charge carriers are transported to and collected by the appropriate electrodes to produce electrical current and/or voltage.[8,9] Compared with silicon-based solar cells, two significant drawbacks have been well described in the literature: low power conversion efficiency (PCE) and inferior stability.[10−12] Focused research has, however, resulted in improvements in both areas. The application of low bandgap polymers and bis-adduct fullerenes,[13−20] for example, in conjunction with optimized casting/annealing procedures,[21−23] has led to OPVs with over 6% power conversion efficiency.[24−26] Recently, an NREL-certified record efficiency of 8.3% was announced by Konarka Technologies, Inc., which suggests that efficiencies as high as 10% may indeed be attainable. With respect to the issue of long-term stability,[27−29] inverted architecture OPVs may represent a viable approach.[30−34] For example, Cheng and co-workers recently reported an unencapsulated inverted OPV retaining 87% of its original 6.22% PCE after 21 days of storage in ambient conditions.[33] Zimmermann and co-workers reported encapsulated inverted OPVs maintaining 90% of the initial efficiency after 1500 h of continuous illumination under a light intensity of ca. 1000 W/m^2 at 50 °C.[34] These and other results suggest that an inverted architecture may provide the ideal solution to solving both the efficiency and stability conundrum in OPVs.

In an inverted OPV device, the indium tin oxide (ITO) acts as the cathode, as shown in Scheme 1. In order to reduce the work function of the ITO to enable its use as the cathode, thin buffer layers of metal oxides or salts such as ZnO, TiO_2, or Cs_2CO_3 are usually deposited onto the ITO.[35−39] Organic compounds are intriguing alternatives because an almost unlimited variety of molecules and polymers with tunable properties are available or can be synthesized. Despite the versatility of an organic molecule-based approach, there are few reports on the use of organic buffer layers for inverted OPVs, particularly with regard to small organic molecules.[40]

Electrostatic layer-by-layer (eLbL) growth is a versatile and efficient approach to the production of compositionally controlled interfacial structures.[41] Via sequential immersion of the substrate in solutions containing cationic and anionic species (such as nanoparticles, polymers, etc), films of controlled thickness and composition can be built up in an efficient fashion.[42,43] Our group has previously exploited hybrid coatings of cationic polythiophenes and anionic poly(3,4-ethylenedioxythiophene):poly(*p*-styrenesulfonate) ($PEDOT:PSS^-$) fabricated by eLbL

Received: June 29, 2011
Accepted: September 27, 2011
Published: September 28, 2011

Scheme 1. Chemical Structures of $(PTCDI^+)I^-$ and $(PEDOT:PSS^-)Na^+$ and the Architecture of Inverted OPVs with ITO Modified by eLbL Assembly of $PTCDI^+$ and $PEDOT:PSS^-$

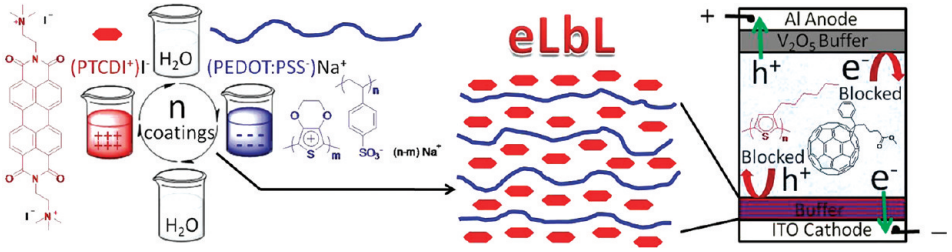

assembly as buffer layers for cathodic ITO in inverted OPVs, with enhanced long-term stability.[43] Herein, we extend this general method to the incorporation of a water-soluble small organic molecule: *N*,*N*′-bis(2-(trimethyl ammonium)ethylene)perylene-3,4,9,10-tetracarboxyldiimide iodide, $(PTCDI^+)I^-$, as shown in Scheme 1. This choice of molecule was based on two considerations: (i) perylenediimide is a typical n-type organic semiconductor with electron transporting and hole blocking properties,[44] and (ii) $PTCDI^+$ has two positively charged ammonium groups that render it soluble in water and allow it to interact with anionic materials in the eLbL process via electrostatic attraction.[45] PEDOT:PSS^- is an aqueous colloidal mixture of cationic poly(3,4-ethylenedioxythiophene) and anionic poly(*p*-styrenesulfonate) with a ratio of 1:6[46] and, hence, bears overall negative charges in water.[43] A series of hybrid films with different numbers of layers were prepared, and their properties relevant to inverted OPV devices were characterized. Employing regioregular 2,5-diyl-poly-(3-hexylthiophene) (P3HT) and [6,6]-phenyl-C_{61}-butyric acid methyl ester (PCBM) as the conventional photoactive materials,[3] devices were fabricated with the following architecture, ITO/$PTCDI^+$:($PEDOT:PSS^-$)/P3HT:PCBM/V_2O_5/Al, and tested in ambient conditions. The performance of inverted OPVs was found to be highly dependent on the number of layers incorporated via eLbL, pointing to the large effect these very thin layers can have on the resulting devices.

2. EXPERIMENTAL SECTION

2.1. Chemicals and Characterization. Perylene-3,4,9,10-tetracarboxylic dianhydride, *N*,*N*-dimethylethylene diamine, methyl iodide, decamethonium bromide, quinoline, toluene, methanol, dichloromethane, isopropyl alcohol, and *o*-dichlorobenzene were purchased from Sigma-Aldrich and used as received. Regioregular P3HT, PCBM, and ($PEDOT:PSS^-$) Na^+ were used as received from Rieke Metals, American Dye Source Inc. and Heraeus (Clevios PVP Al 4083), respectively. ITO coated glass substrates (8−12 Ω $\square^{-1}$, Delta Technologies, Ltd.) were cut into regular pieces with a diamond saw and, then, ultrasonically cleaned for 10 min in each of dichloromethane, water, and isopropyl alcohol. The substrates were further cleaned in a 10 min air plasma (Harrick Plasma, PDC 32G, 18 W) treatment before dip coating. Absorption spectra were obtained with an Agilent 8453 UV−vis spectrometer. NMR spectra were measured with a Varian Inova 400 MHz two-channel spectrometer. Ellipsometry data were obtained with a Gaertner multiangle ellipsometer oriented with a 70° incidence angle, and we assumed negligible absorption at the 632 nm wavelength of the incident laser. Cyclic voltammograms were measured on a Princeton 2273 Potentiostat in a standard three electrode electrochemical cell at a scan rate of 100 mV/s, with Ag/Ag^+ as the reference electrode, a Pt wire as the counter electrode, $(PTCDI^+)I^-$ coated Pt disk (0.071 cm^2) as the working electrode, and 0.1 M Bu_4NPF_6 in acetonitrile as the electrolyte solution. Atomic force microscopy (AFM) images were taken on a Nanoscope IV (Digital Instruments/Veeco) instrument in tapping mode with a Si cantilever (Asylum Research, frequency = 300 kHz). Room temperature X-ray photoelectron spectroscopy (XPS) experiments were performed at the Alberta Centre for Surface Engineering and Science (ACSES) using a Kratos Ultra spectrometer with monochromatized Al Kα (hν = 1486.71 eV) radiation. The spectrometer was calibrated using the binding energy (84.0 eV) of Au 4f7/2 with reference to the Fermi level. The pressure in the analysis chamber during experiments was less than 5×10^{-10} Torr. A hemispherical electron-energy analyzer working at a pass energy of 20 eV was used to collect core-level spectra, and the survey spectrum was collected over the range of binding energies from 0 to 1100 eV using an analyzer pass energy of 160 eV. Charge effects were corrected using the C(1s) peak at 284.8 eV. UV photoelectron spectroscopy (UPS) spectra were measured using He I line irradiation (hν = 21.2 eV). The power for UPS was 3 kV × 10 mA (30 W), and samples were biased at −10 V during measurements to observe the secondary electron edge.

2.2. Preparation of $PTCDI^+$:($PEDOT:PSS^-$) Composite Films. All $PTCDI^+$:($PEDOT:PSS^-$)-coated substrates were formed by aqueous eLbL deposition, as the freshly cleaned ITO coated glass substrates were alternatively dip coated in 0.5 mg/mL aqueous solution of $(PTCDI^+)I^-$ and 0.4 wt % aqueous solution of $(PEDOT:PSS^-)Na^+$. The duration of each immersion was 5 min, and after every immersion, samples were rinsed with deionized water to wash away excess solution. The sample was dipped in modifying solutions *n* times to build up the desired multilayer film with layer number *n*, then spin dried at 3000 rpm for 60 s, and stored in a nitrogen-purged chamber overnight.

2.3. OPV Fabrication and Testing. P3HT (23 mg) and PCBM (23 mg) were separately dissolved in 0.5 mL of *o*-dichlorobenzene and stirred at 65 °C in an inert atmosphere glovebox overnight. They were then mixed together and further stirred for 2 h in the glovebox. The P3HT:PCBM solution was then filtered through 0.2 μm PTFE filters, spin coated at 600 rpm for 60 s on the previously described $PTCDI^+$:-($PEDOT:PSS^-$)-coated ITO/glass substrates, and finally dried in a covered Petri dish for 20 min. Twenty nm of V_2O_5 (Sigma-Aldrich, 99.99%) and 80 nm of Al (Kurt J. Lesker, 99.99%) were thermally evaporated under high vacuum conditions ($\sim 10^{-4}$ Pa) to form complete devices with active areas of 0.2 cm^2. The current−voltage characteristics of completed solar cells were measured using a Keithley 2400 Source Meter, both in the dark and irradiated with a simulated AM 1.5 G spectrum in an Oriel 91191 1000W xenon solar simulator. The solar simulator irradiance was calibrated against an NREL-certified Si reference cell with a PV Measurements, Inc. KG-5 filter (model PVM 624). The irradiance in the range of 200 nm to 20 μm was 140 mW/cm^2. In the range of 200 to 1360 nm, the irradiance was 130 mW/cm^2, and between 300 and 700 nm, the irradiance was 40 mW/cm^2. To test the stability of OPV devices, freshly made devices were tested and stored in air and darkness for 128 days according to the ISOS-D-1 protocol.[47]

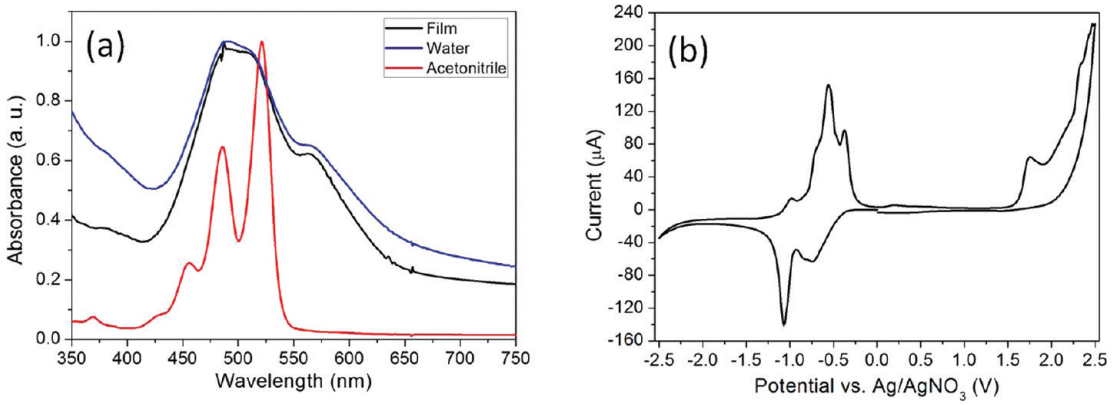

Figure 1. (a) Normalized absorption spectra of dilute $(PTCDI^+)I^-$ solution ($\sim 10^{-5}$ M) in acetonitrile (red) and water (blue) and a $(PTCDI^+)I^-$ film (black). (b) Cyclic voltammogram of a $(PTCDI^+)I^-$ film on a platinum working electrode.

3. RESULTS AND DISCUSSION

3.1. Synthesis and Characterization. $(PTCDI^+)I^-$ has been prepared and studied for a number of applications, including optically active supramolecular ensembles formed in the presence of anionic surfactants,[48−50] chemical sensors for hydrazine and proteins,[51,52] modulation of G-quadruplex conformations in biologically relevant DNA sequences,[53] and antineoplastic agents based on DNA telomerase inhibition.[54] In this study, we exploit the use of $(PTCDI^+)I^-$ as an interfacial material in inverted OPVs to modulate the electronics of the transparent conducting electrode. $(PTCDI^+)I^-$ was synthesized according to literature procedures,[48] and as expected, the material is soluble in water, producing a red aqueous solution (Figure S1, Supporting Information). The normalized absorption spectra of dilute $(PTCDI^+)I^-$ solutions ($\sim 10^{-5}$ M) in acetonitrile and water are displayed in Figure 1a, together with the spectrum of a dried film on a quartz plate. The spectrum of $(PTCDI^+)I^-$ in acetonitrile is typical of a well-dispersed perylenediimide chromophore.[55] The absorption spectra in aqueous solution and the solid state, however, both show a broad peak around 500 nm, a broad shoulder at 565 nm, and absorption onset around 650 nm, features characteristic of perylenediimide aggregates.[45] The cyclic voltammogram of a dried $(PTCDI^+)I^-$ film on a platinum working electrode was measured in acetonitrile and displayed in Figure 1b. In the first scan cycle, the onset reduction and oxidation potentials with respect to $Ag/AgNO_3$ were found to be −0.35 and 1.55 V, respectively. The LUMO and HOMO of $(PTCDI^+)I^-$ film are −4.25 and −6.15 eV, respectively, after calibration using ferrocene as reference. The bandgap is 1.9 eV, matching that calculated from the absorption spectrum. Due to the dissolution of $(PTCDI^+)I^-$ in acetonitrile, subsequent CV cycles are different from the first and resemble the voltammogram of $(PTCDI^+)I^-$ dissolved in acetonitrile solution (Figure S2, Supporting Information).

3.2. eLbL Assembly of $(PTCDI^+)I^-$ with $(PEDOT:PSS^-)Na^+$. Given the positive charges residing on the two ammonium groups in $PTCDI^+$, electrostatic layer-by-layer (eLbL) self-assembly of $PTCDI^+$ with anionic surfactants or polyelectrolytes has been demonstrated in several papers.[45,48−50] In this work, eLbL hybrid films of $PTCDI^+$ and $PEDOT:PSS^-$ were obtained via sequential dip coating as depicted in Scheme 1. After air plasma treatment, the freshly cleaned ITO substrate, which bears an inherent negative charge,[56] was immersed in a 0.5 mg/mL aqueous $(PTCDI^+)I^-$ solution for 5 min and then rinsed thoroughly with deionized water, followed by immersion in an aqueous $(PEDOT:PSS^-)Na^+$ solution for 5 min. The $PTCDI^+$ molecule has a net positive charge, and the $PEDOT:PSS^-$ has a net negative charge; thus, alternation of the immersion steps between cationic and anionic materials leads to the controlled build up of $PTCDI^+$:$(PEDOT:PSS^-)$ multilayers. The byproduct, NaI, is water-soluble and is removed during the rinse steps. An arbitrary number of layers can be built up by performing n immersion steps. In cases where n is even, complete bilayers are formed, and $PEDOT:PSS^-$ is deposited in the final process. In cases where n is an odd number, incomplete bilayers are formed, and cationic $PTCDI^+$ is deposited in the final step.

To demonstrate the efficacy of the eLbL growth of $PTCDI^+$:$(PEDOT:PSS^-)$ films, the optical density of films up to 40 layers (20 bilayers) was measured. The optical density of $PTCDI^+$:$(PEDOT:PSS^-)$ films increased in a linear fashion as depicted in Figure 2a. The strong absorption bands in the 400−650 nm range, together with peaks at 505 nm and shoulders at 550 nm, resemble the features of solid $(PTCDI^+)I^-$ films (Figure 1a). The absorption spectrum of $(PEDOT:PSS^-)Na^+$ was also measured, and no significant absorption peak was found in the 400−650 nm range (Figure S3, Supporting Information). A plot of absorbance at 505 nm versus layer number was constructed (Figure 2b), and the data show a linear relationship between optical density and layer number, attesting to a well-controlled accumulation of thickness. Photographs of ITO substrates coated with n = 0, 8, and 20 layers are shown in the inset of Figure S4, Supporting Information, and these show visual evidence of the buildup of film during the eLbL process. To substantiate the optical density measurements, ellipsometry of $PTCDI^+$:$(PEDOT:PSS^-)$ multilayers formed on silicon substrates also showed a continuous increase of thickness versus layer number (Figure S4, Supporting Information). Atomic force microscopy (AFM) was also performed, and the results are shown in Figure S5, Supporting Information. To investigate the thickness of the layers by AFM, regions of the films were physically removed from the ITO substrates, and the depths of the resulting trench were analyzed by AFM line profiling Figure S5g,h, Supporting Information. For layer numbers of n = 6 and n = 18, average trench depths were around 3.5 and 10.5 nm, respectively.

X-ray photoelectron spectroscopy (XPS) was used to examine the surface composition of the $PTCDI^+$:$(PEDOT:PSS^-)$ films, and the C(1s), N(1s), O(1s), S(2p), Na(1s), and I(3d) regions are shown in Figure 3a−f, respectively. In each of the regions, the spectra for samples with n = 0, 2, 6, 10, and 18 layers are presented. The XPS spectra of neat films of $(PTCDI^+)I^-$ and $(PEDOT:PSS^-)Na^+$ were also measured and shown in Figures S6 and S7 in

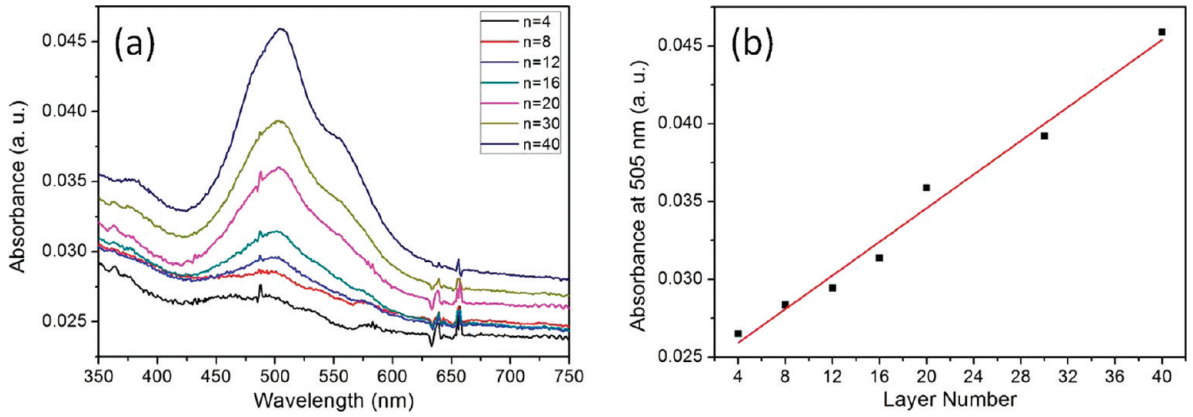

Figure 2. (a) Absorption spectra of $PTCDI^+$:($PEDOT:PSS^-$)-coated quartz with 4, 8, 12, 16, 20, 30, and 40 layers, respectively. (b) The absorbance of modified ITO at 505 nm versus layer number.

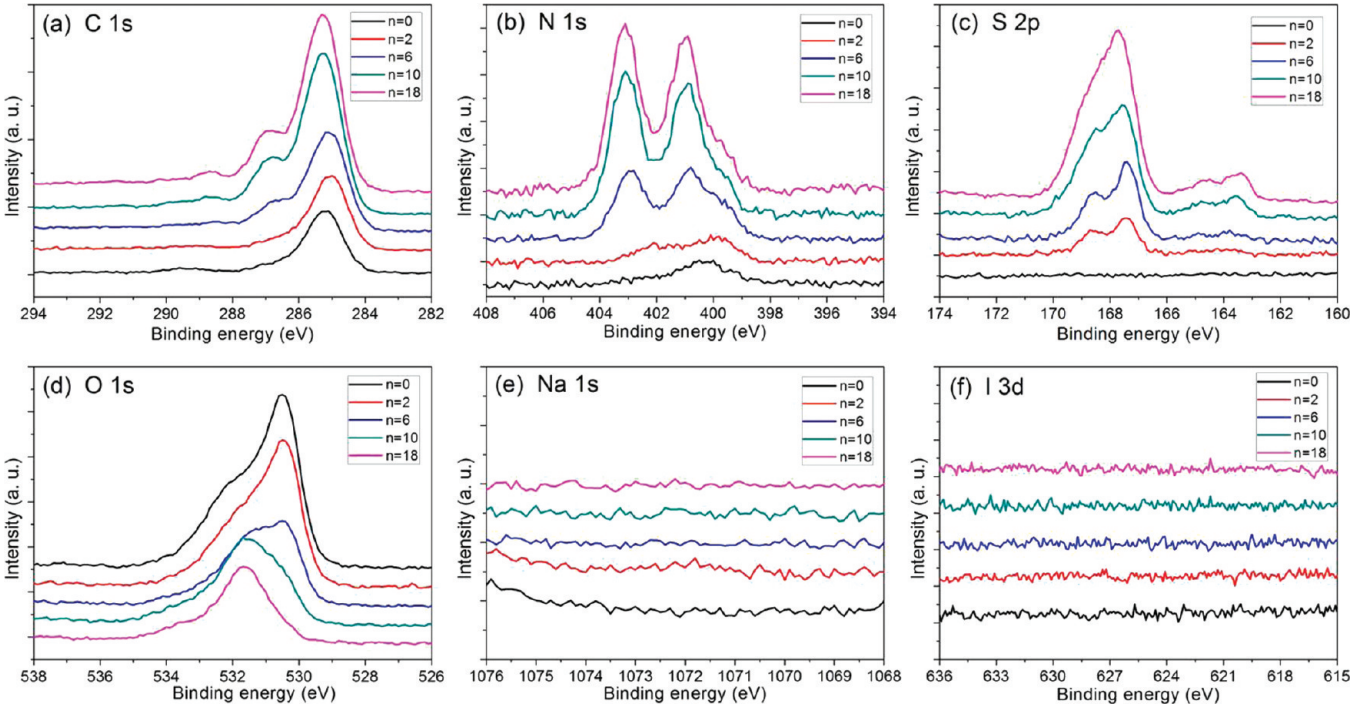

Figure 3. High resolution XPS of the C(1s), N(1s), O(1s), S(2p), Na(1s), and I(3d) regions for $PTCDI^+$:($PEDOT:PSS^-$)-coated ITO with 0, 2, 6, 10, and 18 layers.

the Supporting Information. In Figure 3a, the C(1s) peak intensity at 285 eV increases as layer number increases, indicative of the formation of thicker carbon-containing films. Carbon was also detected in the bare ITO sample because of inevitable contamination when exposed to air. After 6 layers of deposition, a shoulder at 287 eV emerges, which is attributed to the diimide group of $PTCDI^+$ (see Figure S6b, Supporting Information, for comparison). The increasing intensity trend exists in Figure 3b,c as well, where the N(1s) and S(2p) spectra are shown. The increasing peaks at 401 and 403 eV correspond to the diimide and ammonium groups of $PTCDI^+$ (Figure S6c, Supporting Information), respectively, while the increasing peaks at 168 and 164 eV correspond to emission from sulfur atoms in the PSS^- and PEDOT, respectively (Figure S7d, Supporting Information). As seen in Figure 3d, the shift and decrease in the O(1s) peak with increasing thickness of the $PTCDI^+$ and $PEDOT:PSS^-$ hybrid films is due to their lower oxygen content with respect to the underlying ITO substrate. Both the Na(1s) (Figure 3e) and I(3d) (Figure 3f) XPS spectra are featureless, suggesting complete removal of the NaI byproduct. XPS spectra of samples with n = 1, 3, 7, 11, and 19 layers were also measured and show similar trends (Figure S8, Supporting Information). Survey spectra of the above samples are depicted in Figure S9, Supporting Information, and indicate the formation of thicker films with increasing layer number.

Because the surface functionalization is expected to have an influence on the work function of the material, the effect of layer thickness was measured by ultraviolet photoelectron spectroscopy (UPS). As can be seen in Figure 4a, the work function of the surfaces is highly dependent not only on layer thickness but also on whether the $PTCDI^+$ or $PEDOT:PSS^-$ was the top material,

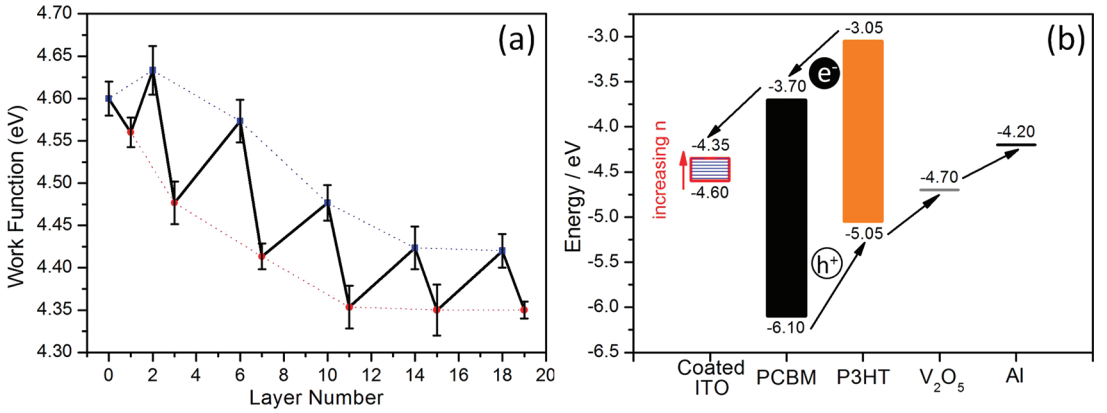

Figure 4. (a) Work function of PTCDI$^+$:(PEDOT:PSS$^-$)-coated ITO as measured by UPS, with 0, 1, 2, 3, 6, 7, 10, 11, 14, 15, 18, and 19 layers. Error bars were calculated on three different measurements. (b) Energy level diagram and charge carrier transport pathway of inverted OPVs with ITO/PTCDI$^+$:(PEDOT:PSS$^-$)/P3HT:PCBM/V_2O_5/Al architecture.

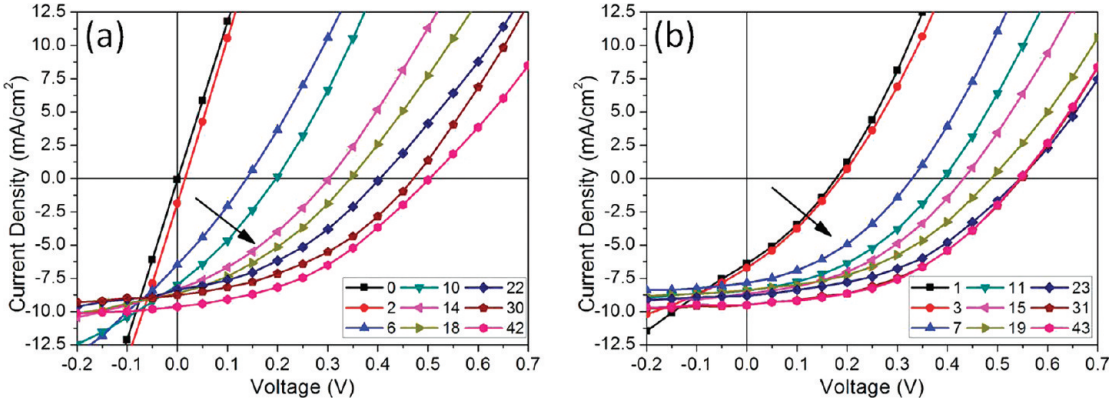

Figure 5. Selected $J-V$ curves of inverted OPVs under illumination with PTCDI$^+$:(PEDOT:PSS$^-$)-coated ITO, where layer numbers are 0, 2, 6, 10, 14, 18, 22, 30, and 42 (a) and 1, 3, 7, 11, 15, 19, 23, 31, and 43 (b). The arrows indicate the direction of increasing layer number.

leading to obvious odd−even effects related to layer number. For raw UPS spectra, see the Supporting Information (Figure S10). When PTCDI$^+$ was the final layer, the measured work function saturated at roughly 4.35 eV (odd n), and when the layer structure ended with PEDOT:PSS$^-$ atop, the work function attained a value of 4.42 eV (even n). The odd−even effect of layer number on the work function is attributed to the differing electronic properties of PTCDI$^+$ and PEDOT:PSS$^-$. As control experiments, the work function of ITO coated with a dried film of (PTCDI$^+$)I$^-$ or (PEDOT:PSS$^-$)Na$^+$ was measured to be 4.32 and 4.75 eV, respectively (Figure S10, Supporting Information).

3.3. Tailored Performance of Inverted OPVs by Layer Number. The measured work functions of PTCDI$^+$:(PEDOT:PSS)$^-$ multilayers, together with the known energy levels of the P3HT:PCBM bulk heterojunction, are plotted in Figure 4b. Incorporation of the V_2O_5 interfacial modifier at the reflective Al contact favors the formation of the inverted OPV arrangement.[35,38] In a working organic solar cell, electrons are transferred downward through LUMO levels, while holes are transferred upward through HOMO levels.[9] Fine control over the work function at the ITO cathode allows the performance of the system to be optimized by varying the layer number, n.

A series of inverted OPVs were constructed with the following architecture: ITO/PTCDI$^+$:(PEDOT:PSS$^-$)/P3HT:PCBM (~200 nm)/V_2O_5 (20 nm)/Al (80 nm). These devices were fabricated and tested under ambient conditions following the same procedures as our previous work.[43] For the PTCDI$^+$:(PEDOT:PSS$^-$) multilayer, layer numbers of 0, 1, 2, 3, 6, 7, 10, 11, 14, 15, 18, 19, 22, 23, 26, 27, 30, 31, 34, 35, 38, 39, 42, and 43 were fabricated and tested. All $J-V$ curves measured in the dark and under illumination are plotted in Figures S11−S22, Supporting Information, and selected $J-V$ curves are plotted in Figure 5. All values of short circuit current (J_{sc}), open circuit voltage (V_{oc}), fill factor (FF), power conversion efficiency (PCE), series resistance (R_s), and shunt resistance (R_{sh}) are listed in Table S1, Supporting Information, and are plotted against layer number in Figure 6. From this data, it is obvious that device performance improves continuously with increasing layer number, and an odd−even effect is observed. Devices with odd layer numbers (red circles) tend to have better performance than their nearest neighbors with even layer numbers (blue squares), and this is true for all six figures of merit. Values of short circuit current, open circuit voltage, fill factor, power conversion efficiency, and shunt resistance increase significantly as layer number increases. For devices with odd layer numbers (PTCDI$^+$ atop), the PCE reaches a limit of ~2.3% after approximately 27 layers, while for devices with even layer numbers (PEDOT:PSS$^-$ atop), the PCE reaches a limit of ca. 1.9% around 38 layers.

To demonstrate the critical role of the conjugated aromatic portion of the PTCDI$^+$ molecule in inverted OPVs, a control experiment was conducted using decamethonium bromide (DAB$^+$)Br$^-$

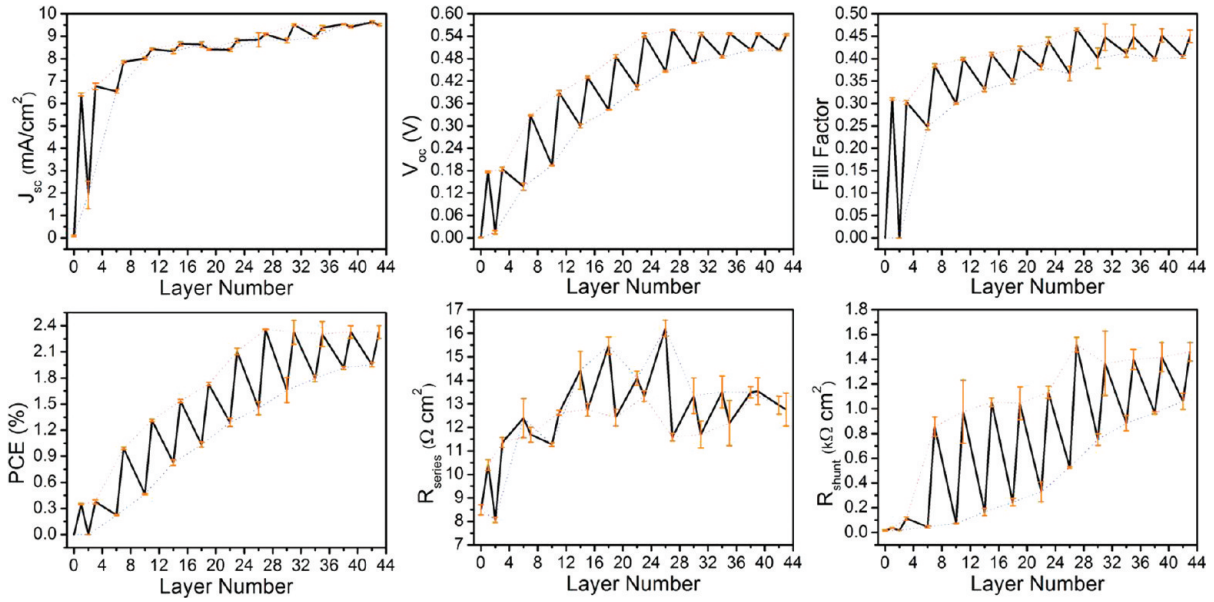

Figure 6. Values of J_{sc}, V_{oc}, FF, PCE, R_s, and R_{sh} for inverted OPVs versus layer number. Error bars were calculated on the basis of five separate measurements.

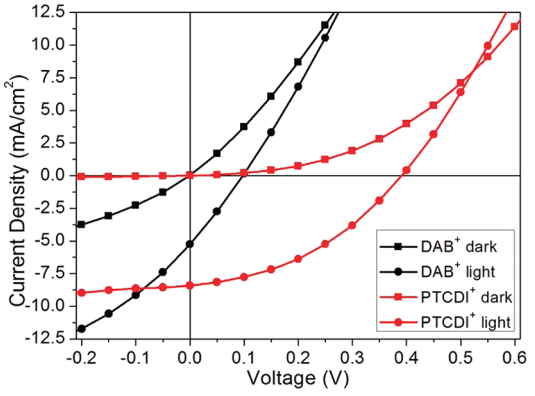

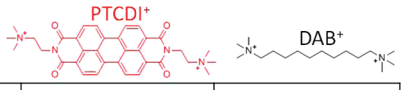

11 layers	PTCDI$^+$:(PEDOT:PSS$^-$)	DAB$^+$:(PEDOT:PSS$^-$)
J_{sc} (mA/cm^2)	-8.43	-5.31
V_{oc} (V)	0.39	0.10
Fill Factor	0.40	0.27
PCE	1.31%	0.16%
R_s (Ω-cm^2)	12.63	11.84
R_{sh} (Ω-cm^2)	977	66

Figure 7. $J-V$ curves of inverted OPVs both in absence of light and under illumination with 11 layers of PTCDI$^+$:(PEDOT:PSS$^-$)- or DAB$^+$:(PEDOT:PSS$^-$)-modified ITO.

in place of (PTCDI$^+$)I$^-$ (Figure 7). DAB$^+$ has two ammonium end groups, like PTCDI$^+$, but in the case of DAB$^+$, these two cationic groups are connected by a saturated alkyl chain. An OPV device with 11 layers of DAB$^+$:(PEDOT:PSS$^-$) on the ITO electrode was fabricated and compared to the corresponding 11 layer PTCDI$^+$:(PEDOT:PSS$^-$) device. As seen from Figure 7, poor OPV performance was observed: the J_{sc} decreased from 8.43 to 5.31 mA/cm^2, the V_{oc} from 0.39 to 0.10 V, the FF from 0.40 to 0.27, the overall PCE from 1.31 to 0.16%, and R_{sh} from 977 to 66 Ω·cm^2, coupled with the appearance of significant dark current. The R_s of both inverted OPVs is close to 12 Ω·cm^2. An additional set of control experiments was conducted using four different hybrid films of 27 dip-coated layers as interfaces for comparison. Twenty-seven layer devices were chosen since, by this point, the power conversion efficiencies had saturated and had therefore reached their maximum. PTCDI$^+$:(PEDOT:PSS$^-$) was contrasted with PTCDI$^+$:PSS$^-$ (a film with no PEDOT:PSS), DAB$^+$:(PEDOT:PSS$^-$) (a film with no PTCDI$^+$), and DAB$^+$:PSS$^-$ (a film with neither PTCDI$^+$ nor PEDOT:PSS). The results are provided in Figure S23 and Table S2, Supporting Information. Both the DAB$^+$:(PEDOT:PSS$^-$) and DAB$^+$:PSS$^-$ hybrid films had very low power conversion efficiencies, while PTCDI$^+$:(PEDOT:PSS$^-$) and PTCDI$^+$:PSS$^-$ films both showed respectable efficiencies, with the former slightly better than the latter, suggesting that the presence of PEDOT does indeed help in improving device performance. The above results can be explained by the fact that perylenediimide acts as n-type semiconductor, transporting electrons and blocking holes, while the saturated alkyl chain is an electrical insulator. Hence, the combination of PTCDI$^+$:(PEDOT:PSS$^-$) or PTCDI$^+$:PSS$^-$ for selective electron collection at the cathode, and V_2O_5 for hole collection at the anode leads to more efficient devices, whereas the combination of DAB$^+$:(PEDOT:PSS$^-$) or DAB$^+$:PSS$^-$ with V_2O_5 lacks an appropriate buffer layer at the cathode and shows inferior performance.

The DAB$^+$ control experiment (Figure 7) showed that perylenediimide, which is reported to be a typical electron acceptor and n-type semiconductor,[44] played a significant role in improving device performance. Hybrid films of PTCDI$^+$:(PEDOT:PSS$^-$)

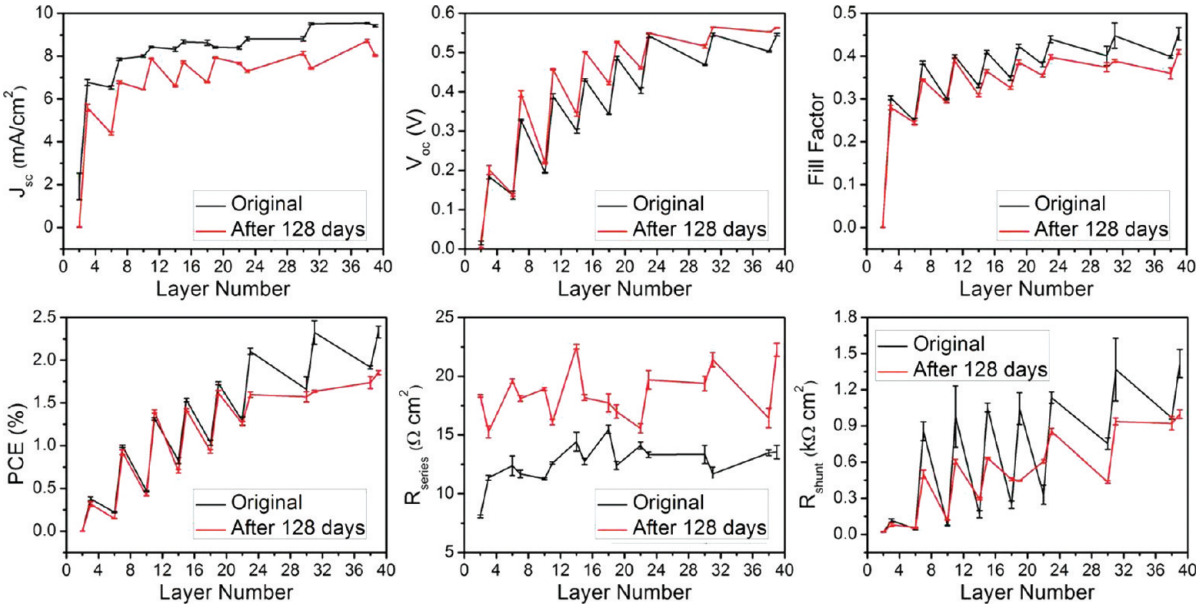

Figure 8. Values of J_{sc}, V_{oc}, FF, PCE, R_s, and R_{sh} of inverted OPVs before and after 128 days of storage in air versus layer number. Error bars were calculated on the basis of five separate measurements.

favor electron transport and act as cathodic buffer layers, in contrast to neat (PEDOT:PSS$^-$)Na$^+$, which is usually used as an anodic buffer layer. The formation of a thicker PTCDI$^+$:-(PEDOT:PSS$^-$) cathodic buffer layer with increasing layer numbers may hamper diffusion of holes to the ITO cathode, leading to a net increase in device performance. The saturation of device performance after a number of layers was possibly due to a balanced state of the above processes at the cathodic buffer layer.

Control over device performance was realized through eLbL engineering of the cathodic interface at a nanometer scale with the combination of PTCDI$^+$ and PEDOT:PSS$^-$. As can be seen from the UPS data, the work function of ITO coated with hybrid films of PTCDI$^+$:(PEDOT:PSS$^-$) was gradually lowered with increasing layer number, and the lowest work functions were measured when PTCDI$^+$ was atop. The decrease of work function, which is the required energy to remove an electron out from the surface of a solid, from 4.6 eV for bare ITO to 4.35 eV for 15 layers of PTCDI$^+$:(PEDOT:PSS$^-$) modified ITO, makes modified ITO a much better cathode for electron extraction. The change of work function is significant as the work function of modified ITO is 0.35 eV lower than that of V_2O_5-coated aluminum, instead of the original 0.1 eV offset. In other words, the reduced work function enhances the polarity of the device, leading to better performance of inverted OPVs. It also minimizes the energy barrier for electron extraction, which is related to the difference of the work function of modified ITO and the LUMO level of PCBM, and increases the energy barrier of hole extraction, which is related to the difference of the work of modified ITO and the HOMO level of P3HT.[32,35] All these factors contributed to the improved device performance as shown in Figure 6.

Finally, the air stability of these inverted cells was measured by retesting them after 128 days of storage in dark ambient condition, as shown in Figure 8. The $J-V$ curves for each device are provided in Figure S24–S31, Supporting Information, and the performance parameters are listed in Table S3, Supporting Information. In Figure 8, the values of J_{sc}, V_{oc}, FF, PCE, R_s, and R_{sh} before and after 128 days of storage in air are plotted versus layer number for comparison, and the ratio of these two sets of values is provided in Figure S32, Supporting Information. As is the case with freshly prepared devices, the performance of aged devices increases with layer number and the odd–even effect persists. The PCE of devices generally decreases after exposure to air, due to the decrease of J_{sc} and FF.[57] As would be expected, a significant increase in R_s is also observed. This degradation of performance may be caused by undesirable reactions at various interfaces, including the donor/acceptor interfaces of the photoactive layer, the photoactive layer and buffer layer, the buffer layer and the electrodes, and the electrode/air.[2,11,58–61] Interestingly, V_{oc} increases instead of decreasing. This observation may be due to the formation of a selective charge carrier transport and collection buffer layer upon exposure to air. Recently, an inverted OPV device was reported to have an increasing V_{oc} during lifetime measurements in air due to the formation of a low resistance and selective contact for charge carriers at the electrode–photoactive layer interface.[62] The mechanistic details with regard to device degradation require additional study and will be the subject of upcoming research. To summarize, almost all inverted OPVs maintained over 70% of their original PCE, and most retained over 90% of their original PCE.

4. CONCLUSION

In summary, a water-soluble organic small molecule, PTCDI$^+$, was used to form composite films with PEDOT:PSS$^-$ through an aqueous solution-based eLbL self-assembly, as confirmed by UV–vis, ellipsometry, XPS, UPS, and AFM techniques. Inverted OPVs with a hybrid film-coated ITO electrode were fabricated and tested under ambient conditions. The device performance was found to be highly dependent on the layer number: a continuous increase in PCE until saturation and an odd–even effect are observed. These results are attributed to the fact that the cationic and n-type semiconductor PTCDI$^+$ is a good cathodic interfacial material for organic photovoltaics. Our experimental results show that both the thickness and composition of buffer layer play significant roles in the

performance of inverted OPVs. The time required to prepare the optimum eLbL interfaces with respect to OPV device performance, those with 27 layers, take over 2 h to prepare since each dip coating step takes 5 min. Reduction of this time may be possible through empirical screening of increased solution concentrations, coupled with modified washing steps; this work will be the subject of an upcoming manuscript. Considering the existence of a large number of water-soluble charged organic semiconductors[63,64] and the convenience of film formation by this aqueous solution eLbL technique, this method represents a simple but general pathway to prepare interfaces for OPVs.[43,65−67]

■ ASSOCIATED CONTENT

Supporting Information. Mass spectra and ^{1}H NMR of $(PTCDI^+)I^-$, cyclic voltammetry, ellipsometry, AFM, XPS, UPS, and $J-V$ curves of OPVs. This material is available free of charge via the Internet at http://pubs.acs.org.

■ AUTHOR INFORMATION

Corresponding Author
*E-mail: jburiak@ualberta.ca.

■ ACKNOWLEDGMENT

This work was supported by the Natural Sciences and Engineering Research Council of Canada (NSERC), NRC-NINT, the University of Alberta School of Energy and the Environment, the Canadian Foundation for Innovation, the Informatics Circle of Research Excellence (iCORE), and Micralyne, Inc. Dr. Dimitre Karpuzov and his colleagues at the Alberta Centre for Surface Engineering and Science (ACSES) are thanked for their considerable assistance with XPS and UPS techniques.

■ REFERENCES

(1) Peet, J.; Heeger, A. J.; Bazan, G. C. *Acc. Chem. Res.* **2009**, *42*, 1700–1708.
(2) Brabec, C. J.; Gowrisanker, S.; Halls, J. J. M.; Laird, D.; Jia, S.; Williams, S. P. *Adv. Mater.* **2010**, *22*, 3839–3856.
(3) Dennler, G.; Scharber, M. C.; Brabec, C. J. *Adv. Mater.* **2009**, *21*, 1323–1338.
(4) Thompson, B. C.; Fréchet, J. M. J. *Angew. Chem., Int. Ed.* **2008**, *47*, 58–77.
(5) Günes, S.; Neugebauer, H.; Sariciftci, N. S. *Chem. Rev.* **2007**, *107*, 1324–1338.
(6) Cai, W.; Gong, X.; Cao, Y. *Sol. Energy Mater. Sol. Cells* **2010**, *94*, 114–127.
(7) Helgesen, M.; Søndergaard, R.; Krebs, F. C. *J. Mater. Chem.* **2010**, *20*, 36–60.
(8) Clarke, T. M.; Durrant, J. R. *Chem. Rev.* **2010**, *110*, 6736–6767.
(9) Blom, P. W. M.; Mihailetchi, V. D.; Koster, L. J. A.; Markov, D. E. *Adv. Mater.* **2007**, *19*, 1551–1566.
(10) Espinosa, N.; Valverde, R. G.; Urbina, A.; Krebs, F. C. *Sol. Energy Mater. Sol. Cells* **2011**, *95*, 1293–1302.
(11) Jorgensen, M.; Norrman, K.; Krebs, F. C. *Sol. Energy Mater. Sol. Cells* **2008**, *92*, 686–714.
(12) Nardes, A. M.; Rupert, B. L.; Larsen, R. E.; Olson, D. C.; Lloyd, M. T.; Shaheen, S. E.; Ginley, D. S.; Rumbles, G.; Kopidakis, N. *Adv. Funct. Mater.* **2010**, *20*, 3476–3483.
(13) Chen, J.; Cao, Y. *Acc. Chem. Res.* **2009**, *42*, 1709–1718.
(14) Liang, Y.; Yu, L. *Acc. Chem. Res.* **2010**, *43*, 1227–1236.
(15) Blouin, N.; Michaud, A.; Gendron, D.; Wakim, S.; Blair, E.; Neagu-Plesu, R.; Belletête, M.; Durocher, G.; Tao, Y.; Leclerc, M. *J. Am. Chem. Soc.* **2008**, *130*, 732–742.
(16) Zou, Y.; Najari, A.; Berrouard, P.; Beaupré, S.; Réda Aích, B.; Tao, Y.; Leclerc, M. *J. Am. Chem. Soc.* **2010**, *132*, 5330–5331.
(17) Boudreault, P. T.; Najari, A.; Leclerc, M. *Chem. Mater.* **2011**, *23*, 456–469.
(18) Chu, T.; Lu, J.; Beaupré, S.; Zhang, Y.; Pouliot, J.; Wakim, S.; Zhou, J.; Leclerc, M.; Li, Z.; Ding, J.; Tao, Y. *J. Am. Chem. Soc.* **2011**, *133*, 4250–4253.
(19) He, Y.; Chen, H.; Hou, J.; Li, Y. *J. Am. Chem. Soc.* **2010**, *132*, 1377–1382.
(20) Lenes, M.; Wetzelaer, G. A. H.; Kooistra, F. B.; Veenstra, S. C.; Hummelen, J. C.; Blom, P. W. M. *Adv. Mater.* **2008**, *20*, 2116–2119.
(21) Zhao, G.; He, Y.; Li, Y. *Adv. Mater.* **2010**, *22*, 4355–4358.
(22) Peet, J.; Senatore, M. L.; Heeger, A. J.; Bazan, G. C. *Adv. Mater.* **2009**, *21*, 1521–1527.
(23) Lee, J. K.; Ma, W. L.; Brabec, C. J.; Yuen, J.; Moon, J. S.; Kim, J. Y.; Lee, K.; Bazan, G. C.; Heeger, A. J. *J. Am. Chem. Soc.* **2008**, *130*, 3619–3623.
(24) Park, S. H.; Roy, A.; Beaupre, S.; Cho, S.; Coates, N.; Moon, J. S.; Moses, D.; Leclerc, M.; Lee, K.; Heeger, A. J. *Nat. Photonics* **2009**, *3*, 297–303.
(25) Son, H. J.; Wang, W.; Xu, T.; Liang, Y.; Wu, Y.; Li, G.; Yu, L. *J. Am. Chem. Soc.* **2011**, *133*, 1885–1894.
(26) Price, S. C.; Stuart, A. C.; Yang, L.; Zhou, H.; You, W. *J. Am. Chem. Soc.* **2011**, *133*, 4625–4631.
(27) Krebs, F. C.; Spanggaard, H. *Chem. Mater.* **2005**, *17*, 5235–5237.
(28) Krebs, F. C.; Norrman, K. *Prog. Photovolt: Res. Appl.* **2007**, *15*, 697–712.
(29) Krebs, F. C. *Sol. Energy Mater. Sol. Cells* **2008**, *92*, 715–726.
(30) Hau, S. K.; Cheng, Y.; Yip, H.; Zhang, Y.; Ma, H.; Jen, A. K. Y. *ACS Appl. Mater. Interfaces* **2010**, *2*, 1892–1902.
(31) Ma, H.; Yip, H.; Huang, F.; Jen, A. K. *Adv. Funct. Mater.* **2010**, *20*, 1371–1388.
(32) Chen, L.; Xu, Z.; Hong, Z.; Yang, Y. *J. Mater. Chem.* **2010**, *20*, 2575–2598.
(33) Cheng, Y.; Hsieh, C.; He, Y.; Hsu, C.; Li, Y. *J. Am. Chem. Soc.* **2010**, *132*, 17381–17383.
(34) Zimmermann, B.; Wurfel, U.; Niggemann, M. *Sol. Energy Mater. Sol. Cells* **2009**, *93*, 491–496.
(35) Li, G.; Chu, C. W.; Shrotriya, V.; Huang, J.; Yang, Y. *Appl. Phys. Lett.* **2006**, *88*, 253503.
(36) Waldauf, C.; Morana, M.; Denk, P.; Schilinsky, P.; Coakley, K.; Choulis, S. A.; Brabec, C. J. *Appl. Phys. Lett.* **2006**, *89*, 233517.
(37) Steim, R.; Choulis, S. A.; Schilinsky, P.; Brabec, C. J. *Appl. Phys. Lett.* **2008**, *92*, 093303.
(38) Liao, H. H.; Chen, L. M.; Xu, Z.; Li, G.; Yang, Y. *Appl. Phys. Lett.* **2008**, *92*, 173303.
(39) White, M. S.; Olson, D. C.; Shaheen, S. E.; Kopidakis, N.; Ginley, D. S. *Appl. Phys. Lett.* **2006**, *89*, 143517.
(40) Motiei, L.; Yao, Y.; Choudhury, J.; Yan, H.; Marks, T. J.; van der Boom, M. E.; Facchetti, A. *J. Am. Chem. Soc.* **2010**, *132*, 12528–12530.
(41) Ariga, K.; Hill, J. P.; Ji, Q. M. *Phys. Chem. Chem. Phys.* **2007**, *9*, 2319–2340.
(42) McClure, S. A.; Worfolk, B. J.; Rider, D. A.; Tucker, R. T.; Fordyce, J. A. M.; Fleischauer, M. D.; Harris, K. D.; Brett, M. J.; Buriak, J. M. *ACS Appl. Mater. Interfaces* **2010**, *2*, 219–229.
(43) Rider, D. A.; Worfolk, B. J.; Harris, K. D.; Lalany, A.; Shahbazi, K.; Fleischauer, M. D.; Brett, M. J.; Buriak, J. M. *Adv. Funct. Mater.* **2010**, *20*, 2404–2415.
(44) Hains, A. W.; Liang, Z.; Woodhouse, M. A.; Gregg, B. A. *Chem. Rev.* **2010**, *110*, 6689–6735.
(45) Weitzel, C. R.; Everett, T. A.; Higgins, D. A. *Langmuir* **2009**, *25*, 1188–1195.
(46) CLEVIOS P VP Al 4083 product information, www.clevios.com (accessed June 2011).

(47) Reese, M. O.; et al. *Sol. Energy Mater. Sol. Cells* **2011**, *95*, 1253–1267.
(48) Huang, Y.; Yan, Y.; Smarsly, B. M.; Wei, Z.; Faul, C. F.J. *J. Mater. Chem.* **2009**, *19*, 2356–2362.
(49) Ma, T.; Li, C.; Shi, G. Q. *Langmuir* **2008**, *24*, 43–48.
(50) Laiho, A.; Smarsly, B. M.; Faul, C. F. J.; Ikkala, O. *Adv. Funct. Mater.* **2008**, *18*, 1890–1897.
(51) Huang, Y. W.; Quan, B. G.; Wei, Z. X.; Liu, G. T.; Sun, L. F. *J. Phys. Chem. C* **2009**, *113*, 3929–3933.
(52) Wang, B.; Yu, C. *Angew. Chem., Int. Ed.* **2010**, *49*, 1485–1488.
(53) Pivetta, C.; Lucatello, L.; Krapcho, A. P.; Gatto, B.; Palumbo, M.; Sissi, C. *Bioorg. Med. Chem.* **2008**, *16*, 9331–9339.
(54) Sissi, C.; Lucatello, L.; Krapcho, A. P.; Maloney, D. J.; Boxer, M. B.; Camarasa, M. B.; Pezzoni, G.; Menta, E.; Palumbo, M. *Bioorg. Med. Chem.* **2007**, *15*, 555–562.
(55) Zhang, X.; Chen, Z.; Wurthner, F. *J. Am. Chem. Soc.* **2007**, *129*, 4886–4887.
(56) Donley, C.; Dunphy, D.; Paine, D.; Carter, C.; Nebesny, K.; Lee, P.; Alloway, D.; Armstrong, N. R. *Langmuir* **2002**, *18*, 450–457.
(57) Voroshazi, E.; Verreet, B.; Aernouts, T.; Heremans, P. *Sol. Energy Mater. Sol. Cells* **2011**, *95*, 1303–1307.
(58) Gevorgyan, S. A.; et al. *Sol. Energy Mater. Sol. Cells* **2011**, *95*, 1398–1416.
(59) Krebs, F. C.; et al. *Sol. Energy Mater. Sol. Cells* **2009**, *93*, 1968–1977.
(60) Norrman, K.; Madsen, M. V.; Gevorgyan, S. A.; Krebs, F. C. *J. Am. Chem. Soc.* **2010**, *132*, 16883–16892.
(61) Norrman, K.; Gevorgyan, S. A.; Krebs, F. C. *ACS Appl. Mater. Interfaces* **2009**, 102–112.
(62) Lloyd, M. T.; Peters, C. H.; Garcia, A.; Kauvar, I. V.; Berry, J. J.; Reese, M. O.; McGehee, M. D.; Ginley, D. S.; Olson, D. C. *Sol. Energy Mater. Sol. Cells* **2011**, *95*, 1382–1388.
(63) Jiang, H.; Taranekar, P.; Reynolds, J. R.; Schanze, K. S. *Angew. Chem., Int. Ed.* **2009**, *48*, 4300–4316.
(64) Huang, F.; Wu, H. B.; Cao, Y. *Chem. Soc. Rev.* **2010**, *39*, 2500–2521.
(65) Hoven, C. V.; Garcia, A.; Bazan, G. C.; Nguyen, T. Q. *Adv. Mater.* **2008**, *20*, 3793–3810.
(66) Mwaura, J. K.; Pinto, M. R.; Witker, D.; Ananthakrishnan, N.; Schanze, K. S.; Reynolds, J. R. *Langmuir* **2005**, *21*, 10119–10126.
(67) Masuda, K.; Abe, T.; Benten, H.; Ohkita, H.; Ito, S. *Langmuir* **2010**, *26*, 13472–13478.